Second Harmonic Emission From Dielectric Nanoresonators in the Absorption Regime

Andrea Tognazzi, Paolo Franceschini, Davide Rocco, Luca Carletti, *Member, IEEE*, Andrea Locatelli, *Member, IEEE*, Marco Gandolfi, Dario Zappa, Alfonso Carmelo Cino, Elisabetta Comini, Giuseppe Leo, and Costantino De Angelis

***Abstract*— We study second harmonic generation in dielectric nanocylinders as a function of the wavelength of the incident field and geometrical dimensions. Uncommonly, we consider a spectral range in which the emitted nonlinear signal is partially absorbed by the dielectric. Surprisingly, we reveal that the second harmonic efficiency does not decrease as the imaginary part of the complex dielectric refractive index increases. Indeed, the presence of higher order multipoles supported by the resonators at the fundamental wavelength can significantly boost the generated second harmonic signal even in the dielectric absorption spectral region achieving nonlinear efficiency of the same order of magnitude with respect to the lossless case.**

***Index Terms*— Second harmonic generation, absorption, nanoresonators, dielectric.**

I. Introduction

SUB-WAVELENGTH nanoresonators made of dielectric materials possess a plethora of optical resonances allowing local intensity enhancement, electromagnetic field confinement and emitted radiation shaping [1], [2], [3], [4]. Recently, the spatial repetition of such nano-elements has allowed to realize thin devices – also named metasurfaces – with remarkable light manipulation properties [5], [6], [7], [8]. In particular, geometrical parameters (*i.e.*, shape and dimension) of the resonator itself strongly influence the optical response, which is typically described as a superposition of Mie-type resonances [9], [10], [11]. Magnetic and electric dipolar modes, together with higher order modes, have opened a new way to boost the nonlinear optical generation in nanophotonic devices [12], [13], [14], [15], [16], [17]. Moreover, the strong light–matter interaction in such systems paves the way for a dynamic control of the nonlinear harmonic response via alteration of optical or geometrical properties [18], [19], [20], [21], [22], [23], [24], [25], [26], [27]. Future applications such as optical detection, imaging, holography, quantum communication and computing, virtual or augmented reality, strongly motivated the study of reconfigurable metasurfaces with nonlinear modulation frequencies ranging from kHz to GHz [28]. In this context, efficient optically-induced modulation of the Second Harmonic (SH) generation in AlGaAs nanodisks has recently been demonstrated by exploiting the thermo-optical effect, achieved by illuminating the nano-objects with an additional continuous-wave laser beam in proximity of the material bandgap wavelength (*i.e.*, in the material absorption region) [29]. Moreover, in [30] a dielectric metasurfaces for enhanced second-harmonic generation using Gallium Arsenide (GaAs) is designed by optimizing solely dipolar resonances at the fundamental frequencies with absorption that occurs at the SH wavelengths which are shorter than the GaAs bandgap. Instead, in [31] the role of absorption losses in GaAs nanowire in SH generation is theoretically discussed. However, the majority of demonstration in the field focus on the case where both pump and emission wavelengths are in the transparency band of the resonator material.

Our work demonstrates that, in spite of the presence of absorption, SH conversion efficiency from $Al_{0.18}Ga_{0.82}As$ nanodisk in the visibile region can be comparable to previous results where the nonlinear signal is radiated in the near infrared region, *i.e.*, in the absence of losses. Notably, for specific resonator dimensions, we demonstrate that the SH emitted at 625 nm, where a magnetic quadrupolar resonance is excited at the Fundamental Wavelength (FW), is of the same order of magnitude as the one observed at 900 nm, where a magnetic dipole is excited at the FW. The possibility to generate nonlinear signals in the visible range with acceptable efficiency may extend the capabilities of platforms based on AlGaAs nanostructures in several fields such as sensing, imaging and holography.

Manuscript received 3 February 2023; revised 6 March 2023; accepted 21 March 2023. Date of publication 23 March 2023; date of current version 3 April 2023. This work was supported in part by the European Commission under Grant 899673 and Grant FETOPEN-01-2018-2019-2020; in part by Consiglio Nazionale delle Ricerche (Joint Laboratories Program) under Grant SAC.AD002.026; and in part by Ministero dell'Istruzione, dell'Università e della Ricerca [Progetto di Rilevante Interesse Nazionale (PRIN) NOnlinear photonics with MEtal-less Nanoantennas and metasurfaces (NOMEN)] under Grant 2017MP7F8F. The work of Andrea Tognazzi and Marco Gandolfi was supported by the European Union through "FESR o FSE, Programma Operativo Nazionale (PON) Ricerca e Innovazione" 2014–2020 under Grant DM 1062/2021. *(Corresponding author: Davide Rocco.)*

Andrea Tognazzi and Alfonso Carmelo Cino are with the Department of Engineering, University of Palermo, 90128 Palermo, Italy.

Paolo Franceschini is with Consiglio Nazionale delle Ricerche, Istituto Nazionale di Ottica, 25123 Brescia, Italy.

Davide Rocco, Luca Carletti, Andrea Locatelli, Marco Gandolfi, and Costantino De Angelis are with the Department of Information Engineering, University of Brescia, 25123 Brescia, Italy, also with Consiglio Nazionale delle Ricerche, Istituto Nazionale di Ottica, 25123 Brescia, Italy, and also with Consorzio Interuniversitario per le Telecomunicazioni, 43124 Parma, Italy (e-mail: davide.rocco@unibs.it).

Dario Zappa and Elisabetta Comini are with the Department of Information Engineering, University of Brescia, 25123 Brescia, Italy.

Giuseppe Leo is with the Matériaux et Phénomènes Quantiques, Université Paris Cité, 75014 Paris, France.

Color versions of one or more figures in this letter are available at https://doi.org/10.1109/LPT.2023.3260878.

Digital Object Identifier 10.1109/LPT.2023.3260878

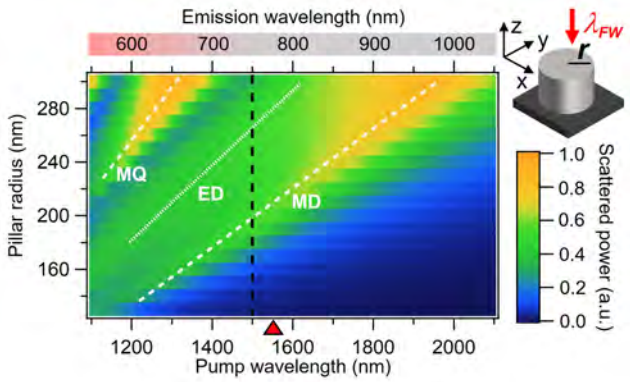

Fig. 1. The scattered power as a function of the incident pump wavelength for different pillar radius, r. The dotted white lines represent the MQ, ED and MD dispersion curves, whereas the dotted black line denotes the border beyond which the absorption at the SH wavelength is not negligible (*i.e.* below 750 nm). The red triangle indicates the commonly used wavelength of 1550 nm.

II. Theoretical Analysis

First, we investigate the optical response of $Al_{0.18}Ga_{0.82}As$ nanocylinders in the near infrared region via finite element method simulations performed in Comsol Multiphysics. To this purpose, we consider $Al_{0.18}Ga_{0.82}As$ nanodisks placed over an AlOx substrate ($n = 1.6$) with increasing radii, r, ranging from 130 nm to 300 nm and fixed height equal to 400 nm. The AlGaAs [100] crystalline axis is aligned along the x-axis. By assuming an x-linearly polarized plane wave with an intensity I_0 =1 GW/cm^2 and wavelength λ_{FW} as the impinging electromagnetic source on the AlGaAs sample, we obtain the linear behavior (scattered power) reproduced in Fig. 1. The excitation is coming from the air towards the substrate. Multipolar decomposition [32] allows to demonstrate that, in the considered frequency range, the light scattered from smaller nanodisks (up to $r = 210$ nm) is governed by a mingling of magnetic (MD) and electric dipolar (ED) resonance with a dominant MD contribution, whereas for nanodisks with larger radii also a magnetic quadrupolar (MQ) resonance is excited at shorter wavelength. We point out that both the dominant MD and MQ contributions can be excited at the FW for the selected geometrical parameters with comparable field enhancement inside the nanodisk. At this stage, we stress that for fundamental wavelength higher than 1500 nm, the AlGaAs losses can be considered negligible both at the FW and the emission one, λ_{SH}. For nanodisk radii larger than 200 nm, the MD resonance falls into this regime. On the contrary, regarding the MQ resonance, the losses at the SH wavelength cannot be neglected. Hence, we proceed to quantify the impact of losses at λ_{SH} in SHG process for the two aforementioned different cases.

As a reference, let us focus on a nanodisk with $r = 260$ nm which is the smallest resonator, in the considered window, that supports MD and MQ resonances with equivalent scattered efficiency. Moreover, for this pillar, the MD resonance falls in the non-absorption regime whereas the MQ is in the absorption regime at λ_{SH}. Fig. 2(a) shows the scattered power of the pillar with $r = 260$ nm and the field distribution related to the two main resonances. To evaluate the effect of losses at λ_{SH} in

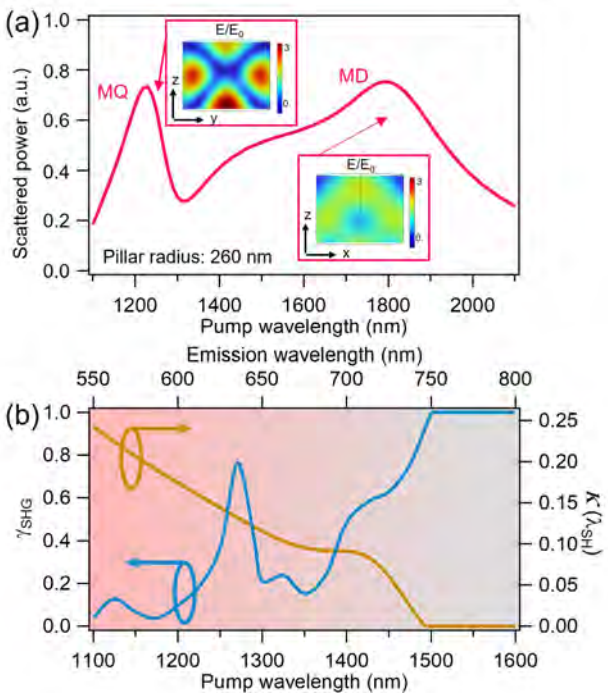

Fig. 2. (a) Scattered power as a function of the incident pump wavelength for the pillar with radius 260 nm. The insets show the field distribution at the MQ ($\sim$ 1250 nm) and MD ($\sim$ 1800 nm) resonances. (b) The γ_{SHG} parameter as a function of the incident wavelength evaluated for the nanodisk with radius of 260 nm (left axis, blue curve) in comparison with the imaginary part of the complex AlGaAs refractive index (right axis, brown curve) as a function of the emission wavelength. The values of the top axis (emission wavelength) are half of those of the bottom one (pump wavelength).

the nonlinear generation of the second harmonic, we define γ_{SHG} as:

$$\gamma_{SHG} = \frac{P^{SHG}[\kappa(\lambda_{SH})]}{P^{SHG}[\kappa = 0]} \tag{1}$$

where $P^{SHG}[\kappa(\lambda_{SH})]$ is the emitted SH power captured by an objective with Numerical Aperture, NA = 0.85, and $\kappa(\lambda_{SH})$ is the imaginary part of the AlGaAs refractive index at the second harmonic wavelength, while $P^{SHG}[\kappa = 0]$ represents the emitted SH power in the same objective when the losses at the emission wavelength are artificially set to zero.

We perform nonlinear simulations to evaluate P^{SHG} following the well-known approach based on nonlinear current densities adopted in [12] and we report the obtained results in Fig. 2(b). We note that, in absence of losses, γ_{SHG} is always equal to 1 by definition. In more detail, the blue curve of Fig. 2(b) refers to γ_{SHG} for the selected nanodisk with $r = 260$ nm. For comparison, the brown curve represents the imaginary part of the complex refractive index at the SH emission wavelength, $\kappa(\lambda_{SH})$. As expected, for emission wavelengths larger than 750 nm, $\gamma_{SHG} = 1$ since $\kappa = 0$ for AlGaAs in this frequency range. Importantly, one can notice that the γ_{SHG} trend is not monotonic and not inversely proportional to κ. Around 1250 nm, which is the pump wavelength at which the MQ is excited, γ_{SHG} reaches is maximum value of 0.75. In other words, in the correspondence of the MQ, 75% of the potential SH power is actually emitted. This results in a moderately high SH efficiency. Indeed,

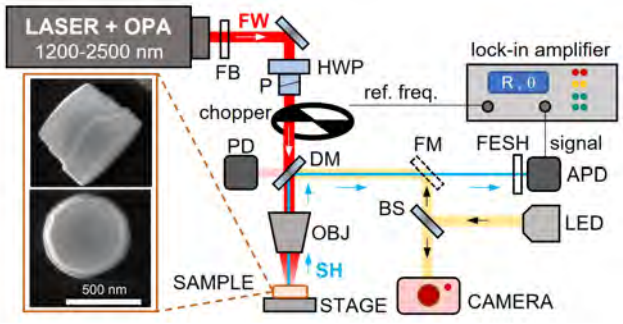

Fig. 3. Sketch of the experimental set-up. The inset shows a SEM image of one of the fabricated pillar. OPA: optical parametric amplifier; FB: bandpass filter; HWP: half-wave plate, P: polarizer; PD: photodiode; DM: dichroic mirror; FM: flip mirror; FESH: shortpass filter; APD: avalanche photodiode; BS: beam-splitter; OBJ: objective.

around the MQ resonance, we achieve a SH efficiency of $5.22 \cdot 10^{-8}$ (NA $= 0.85$, I_0=1 GW/cm^2) while around the MD resonance, for an incident wavelength of 1800 nm, the nonlinear efficiency is $8 \cdot 10^{-8}$ (i.e. a factor 1.54 higher). In the previous calculations, we apply the same definition of SH efficiency as reported in [12]. The modal overlap with the mode induced at the second harmonic for the MD is about 68% whereas is 74% for the MQ [33].

III. Experimental Results and Discussion

To validate and verify our theoretical prediction, we fabricated several pillars with various radii in the 130-300 nm range, following the same fabrication procedures as in [12]. The actual size of the pillar radius was retrieved by Scanning Electron Microscopy (TESCAN Field Emission SEM, MIRA 3 model) images, as the ones shown in Fig. 3. The SH signal generated by single nanopillars was measured employing the setup sketched in Fig. 3. A fiber laser (Coherent Monaco, 1035 nm wavelength, 1 MHz repetition rate) pumps an optical parametric amplifier (OPA, Coherent Opera-F), which delivers a coherent beam with tunable wavelength in the infrared (1200-2500 nm), with $\sim$ 100 nm bandwidth (full-width at half maximum, FWHM). The spectral content of the beam at FW is further selected by employing a band pass filter (Thorlabs FB1XX0-12 series) to select a 12 nm large bandwith (FWHM) around the central wavelength. An half-waveplate (Thorlabs AHWP10M-1600) and a polarizer (Thorlabs GL10) are used to control the impinging intensity of the FW beam (monitored by a photodiode, Thorlabs DET05D2), which is focused down to 1-μm-size (beam waist) on the sample surface by an objective (Olympus NIR 100x NA=0.85). A 3-axis stage (SmarAct MCS2) allows to control the sample position with a spatial resolution of less than 100 nm; moreover, an imaging system based on a LED (Thorlabs MWWHL4) and a CCD camera (Thorlabs CS2100M-USB) are used to verify the proper overlap between the laser spot and the nanodisk. After the interaction with the sample, the reflected beams at FW and SH are separated by a dichroic mirror (Thorlabs DMLP950). An additional short pass filter (Thorlabs FESH900) is inserted to remove unwanted reflections at FW from the SH beam, which is focused onto an avalanche silicon detector (Thorlabs

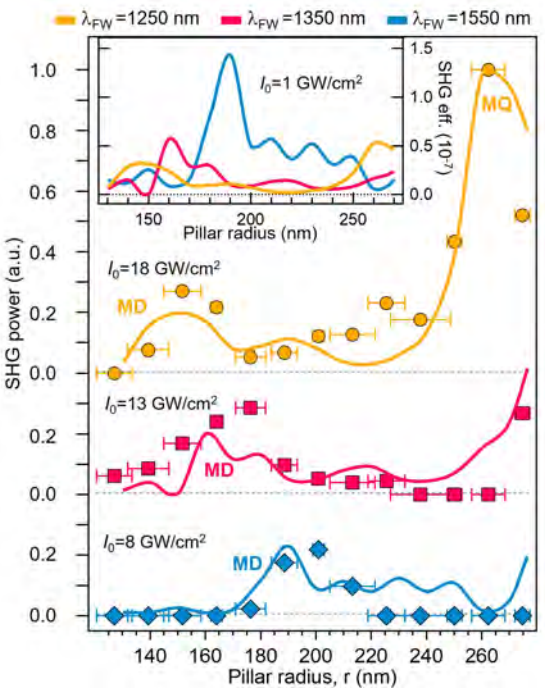

Fig. 4. The comparison between experimental (markers) and simulated (continuous lines) SHG power as a function of the pillar radius, for three different incident wavelengths and pump intensities. The inset displays the simulated SHG efficiency for pump with fixed intensity (1 GW/cm^2) for the three λ_{FW} values used in the main panel, NA $= 0.85$.

APD410A/M). Given the low-level intensity of the SH beam, the detection is performed with a lock-in amplifier (Ametek Signal Recovery DSP 7230). To this purpose, the beam at FW is modulated by a chopper wheel before reaching the sample.

To quantify the SHG emitted power when losses are present, in the experiment, we vary the pump wavelength to excite the MQ in the nanodisk with radius equal to 260 nm. The measured SH power is reported in Fig. 4 (marker). We increase the pump intensity at shorter wavelength to appreciate the second harmonic generated at the MD resonance. The comparison with the numerical simulations, Fig. 4 (line), is qualitatively good and confirms our theoretical predictions. Around the MQ it is possible to observe a SH peak, even if the emitted radiation is partially absorbed. For completeness, the inset of Fig. 4 reports the SHG efficiency as a function of the nanodisk radius for the three considered pump wavelengths, at the same pump intensity. In our previous work, we have already verified that, in the considered spectral and geometrical window, the maximum SHG efficiency is reached for a pillar of radius 190 nm at 1550 nm around its MD resonance [12]. For this reason, to obtain the fairest comparison, we consider the pillar with $r = 190$ nm as the best-case scenario for the excitation of the MD resonance. Although, as expected, the SH efficiency peak is reached for a pillar with $r = 190$ nm around the MD mode, a noticeable peak is also achieved when $r = 260$ nm at the MQ resonance. Please note that the SHG efficiency emitted from the pillar with $r = 260$ nm around its MQ resonance is reduced by a factor of 2.68 with respect to the one coming from the optimal pillar with $r = 190$ nm at the MD resonance. However, if we compare the SHG efficiency from the same

pillar ($r = 260$ nm), we observe a reduction of a factor of 1.54 when the pump is tuned to the MQ respect to the MD. This limited reduction in the SHG efficiency is mainly due to the higher intensity enhancement of the MQ resonance with respect to the MD. Finally, let us underline that no significant differences are observed in the simulated SH power when the surface nonlinearities are also considered [34].

IV. Conclusion

We have studied SH emission from AlGaAs nanodisks when the nonlinear signal is emitted in the dielectric absorption regime. By exploiting magnetic quadrupolar resonances at FW in the lossless region, we generated SH in the visible range (with absorption), with conversion efficiencies on the same order as those provided by magnetic dipolar resonances previously employed in the near infrared region. Our work may open new possibilities in view of the realization of tunable nonlinear metasurfaces exploiting higher order modes to generate nonlinear signal beyond the material transparency window.

References

[1] A. E. Krasnok, A. E. Miroshnichenko, P. A. Belov, and Y. S. Kivshar, "All-dielectric optical nanoantennas," *Opt. Exp.*, vol. 20, no. 18, pp. 20599–20604, 2012.

[2] A. I. Kuznetsov, A. E. Miroshnichenko, M. L. Brongersma, Y. S. Kivshar, and B. Luk'yanchuk, "Optically resonant dielectric nanostructures," *Science*, vol. 354, no. 6314, Nov. 2016, Art. no. aag2472.

[3] A. E. Krasnok et al., "Optical nanoantennas," *Phys.-Usp.*, vol. 56, no. 6, p. 539, Jun. 2013.

[4] I. S. Maksymov, I. Staude, A. E. Miroshnichenko, and Y. S. Kivshar, "Optical yagi-uda nanoantennas," *Nanophotonics*, vol. 1, no. 1, pp. 65–81, Jul. 2012.

[5] Y. Yu, A. Zhu, R. Paniagua-Domínguez, Y. Fu, B. Luk'yanchuk, and A. I. Kuznetsov, "High-transmission dielectric metasurface with 2Π phase control at visible wavelengths," *Laser Photon. Rev.*, vol. 9, no. 4, pp. 412–418, Jul. 2015.

[6] A. Zhan, S. Colburn, R. Trivedi, T. K. Fryett, C. M. Dodson, and A. Majumdar, "Low-contrast dielectric metasurface optics," *ACS Photon.*, vol. 3, no. 2, pp. 209–214, Feb. 2016.

[7] Z. Wang, T. Li, A. Soman, D. Mao, T. Kananen, and T. Gu, "On-chip wavefront shaping with dielectric metasurface," *Nature Commun.*, vol. 10, no. 1, pp. 1–7, Aug. 2019.

[8] A. Tognazzi et al., "Third-harmonic light polarization control in magnetically resonant silicon metasurfaces," *Opt. Exp.*, vol. 29, no. 8, p. 11605, 2021.

[9] W. Yang et al., "All-dielectric metasurface for high-performance structural color," *Nature Commun.*, vol. 11, no. 1, pp. 1–8, Apr. 2020.

[10] P. Genevet, F. Capasso, F. Aieta, M. Khorasaninejad, and R. J. O. Devlin, "Recent advances in planar optics: From plasmonic to dielectric metasurfaces," *Optica*, vol. 4, no. 1, pp. 139–152, 2017.

[11] D. Rocco, A. Lamprianidis, A. E. Miroshnichenko, and C. De Angelis, "Giant electric and magnetic Purcell factor in dielectric oligomers," *J. Opt. Soc. Amer. B, Opt. Phys.*, vol. 37, no. 9, pp. 2738–2744, 2020.

[12] V. F. Gili et al., "Monolithic AlGaAs second-harmonic nanoantennas," *Opt. Exp.*, vol. 24, no. 14, pp. 15965–15971, 2016.

[13] H. K. Gandhi, D. Rocco, L. Carletti, and C. De Angelis, "Gain-loss engineering of bound states in the continuum for enhanced nonlinear response in dielectric nanocavities," *Opt. Exp.*, vol. 28, no. 3, pp. 3009–3016, 2020.

[14] G. Marino et al., "Harmonic generation with multi-layer dielectric metasurfaces," *Nanophotonics*, vol. 10, no. 7, pp. 1837–1843, May 2021.

[15] A. Zilli et al., "Frequency tripling via sum-frequency generation at the nanoscale," *ACS Photon.*, vol. 8, no. 4, pp. 1175–1182, Apr. 2021.

[16] K. I. Okhlopkov et al., "Tailoring third-harmonic diffraction efficiency by hybrid modes in high-Q metasurfaces," *Nano Lett.*, vol. 21, no. 24, pp. 10438–10445, Dec. 2021.

[17] J. Yu et al., "Electrically tunable nonlinear polaritonic metasurface," *Nature Photon.*, vol. 16, no. 1, pp. 72–78, Jan. 2022.

[18] D. Rocco et al., "Opto-thermally controlled beam steering in nonlinear all-dielectric metastructures," *Opt. Exp.*, vol. 29, no. 23, pp. 37128–37139, 2021.

[19] D. Rocco et al., "Tunable second harmonic generation by an all-dielectric diffractive metasurface embedded in liquid crystals," *New J. Phys.*, vol. 24, no. 4, Apr. 2022, Art. no. 045002.

[20] E. A. A. Pogna et al., "Ultrafast, all optically reconfigurable, nonlinear nanoantenna," *ACS Nano*, vol. 15, no. 7, pp. 11150–11157, Jul. 2021.

[21] T. Liu, X. Fang, and S. Xiao, "Tuning nonlinear second-harmonic generation in AlGaAs nanoantennas via chalcogenide phase-change material," *Phys. Rev. B, Condens. Matter*, vol. 104, no. 19, Nov. 2021, Art. no. 195428.

[22] S. V. Makarov et al., "Light-induced tuning and reconfiguration of nanophotonic structures," *Laser Photon. Rev.*, vol. 11, no. 5, Sep. 2017, Art. no. 1700108.

[23] C. Zou, J. Sautter, F. Setzpfandt, and I. Staude, "Resonant dielectric metasurfaces: Active tuning and nonlinear effects," *J. Phys. D, Appl. Phys.*, vol. 52, no. 37, Sep. 2019, Art. no. 373002.

[24] A. M. Shaltout, V. M. Shalaev, and M. L. Brongersma, "Spatiotemporal light control with active metasurfaces," *Science*, vol. 364, no. 6441, May 2019, Art. no. eaat3100.

[25] Q. He, S. Sun, and L. Zhou, "Tunable/reconfigurable metasurfaces: Physics and applications," *Research*, vol. 2019, pp. 1–16, Jan. 2019.

[26] C.-W. Lee, H. J. Choi, and H. Jeong, "Tunable metasurfaces for visible and SWIR applications," *Nano Converg.*, vol. 7, no. 1, pp. 1–11, Dec. 2020.

[27] L. Carletti, D. de Ceglia, M. Vincenti, and C. De Angelis, "Self-tuning of second-harmonic generation in GaAs nanowires enabled by nonlinear absorption," *Opt. Exp.*, vol. 27, no. 22, pp. 32480–32489, 2019.

[28] L. Carletti et al., "Reconfigurable nonlinear response of dielectric and semiconductor metasurfaces," *Nanophotonics*, vol. 10, no. 17, pp. 4209–4221, Nov. 2021.

[29] M. Celebrano et al., "Optical tuning of dielectric nanoantennas for thermo-optically reconfigurable nonlinear metasurfaces," *Opt. Lett.*, vol. 46, no. 10, pp. 2453–2456, 2021.

[30] S. Liu et al., "Resonantly enhanced second-harmonic generation using III—V semiconductor all-dielectric metasurfaces," *Nano Lett.*, vol. 16, no. 9, pp. 5426–5432, 2016.

[31] D. de Ceglia, L. Carletti, M. A. Vincenti, C. De Angelis, and M. Scalora, "Second-harmonic generation in mie-resonant GaAs nanowires," *Appl. Sci.*, vol. 9, no. 16, p. 3381, Aug. 2019.

[32] P. Grahn, A. Shevchenko, and M. Kaivola, "Electromagnetic multipole theory for optical nanomaterials," *New J. Phys.*, vol. 14, no. 9, Sep. 2012, Art. no. 093033.

[33] L. Carletti, A. Locatelli, O. Stepanenko, G. Leo, and C. De Angelis, "Enhanced second-harmonic generation from magnetic resonance in AlGaAs nanoantennas," *Opt. Exp.*, vol. 23, no. 20, pp. 26544–26550, 2015.

[34] S. D. Gennaro et al., "Cascaded optical nonlinearities in dielectric metasurfaces," *ACS Photon.*, vol. 9, no. 3, pp. 1026–1032, Mar. 2022.

Open Access funding provided by 'Università degli Studi di Brescia' within the CRUI CARE Agreement